Enabling WiGig Communications Using Quantum-Dash Laser Source Under Smoky Weather Conditions

Amr M. Ragheb, Q. Tareq, Maged. A. Esmail, Muhammad R. Alrabeiah, *Member, IEEE*, Saleh. A. Alshebeili, and Mohammed Z. M. Khan, *Senior Member, IEEE*

***Abstract*—Wireless Gigabit (WiGig) is a recent wireless local area network that operates at the 60-GHz band and supports a transmission data rate of up to 20 Gbps. This paper demonstrates the generation of a V-band millimeter-wave (mmWave) signal using a new class of InAs/InP quantum-dash laser-based comb source operating in the L-band region. A 62.5-GHz mmWave signal is generated with electrical linewidth and phase noise characterization of 1 kHz and −65 dBc/Hz, respectively. Then, the transmission of the 6-Gbaud quadrature phase-shift keying (12 Gbps) signal is experimentally achieved over a hybrid radio-over-fiber (RoF) and radio-over-free-space (RoFSO) architecture comprising an 11.6-km single-mode fiber (SMF), 6-m FSO, and up to 2-m wireless link. Moreover, we also report this WiGig signal's transmission performance in terms of the measured bit error rate and error vector magnitude under various density smoke FSO channels, exhibiting a visibility range of ∼100 m for error-free transmission.**

***Index Terms*—InAs/InP quantum-dash laser diode, mmWave, RoF, RoFSO, WiGig, L-band.**

I. Introduction

THE rapidly growing data traffic is a defining landscape for today's world. This is a consequence of the increasing number of internet users, which is projected to experience an approximately 36% growth by 2023 over the number of users in 2018 [1]. What is interesting about the projection is that it also estimates a significant contribution from machines to the overall traffic; machine-to-machine (M2M) connection is expected to represent half of the connected devices by 2023. These projections are not surprising, for they result from the continuously growing interest in data-hungry applications like 8 K video streaming and Virtual/Augmented Reality (VR/AR) as well as technologies with the massive machine-type connection such as the Internet of Things (IoT).

A downside of the projected accelerating growth in data traffic is that it needs to be matched with wireless communication systems and networks capable of meeting the demands for data and services. With the abundance of bandwidth available in the millimeter-wave (mmWave) spectrum, mmWave systems and networks are envisioned as one promising solution to shoulder the burden of that traffic [2], [3]. Wireless Gigabit (WiGig), standards IEEE 802.11ad and IEEE 802.11ay, is an excellent example of mmWave systems that attempts to meet those traffic demands. It operates in the 60 GHz band and offers a vast bandwidth of roughly 14 GHz. This makes it capable of providing Giga-bit per second (Gbps) data rates, e.g., up to 8 Gbps for IEEE 802.11 ad and up to 100 Gbps for IEEE 802.11 ay. Hence, serve the growing number of users [4] and enables applications such as high-speed video streaming and data transfer [5]. Besides, beamforming technology, at this band, encourages the utilization of WiGig signals to demonstrate beam-focused applications such as device-to-device communications [6] and crowd management [7].

Although WiGig has the potential to support the growing data traffic, its reliance on the mmWave spectrum brings about new deployment challenges, one of the most important of which is the short-range propagation [8]. This is a result of the propagation characteristics of signals in the mmWave range and, especially, the 60-GHz band [2]. Particularly, Oxygen molecules cause intrinsic atmospheric attenuation of 15 dB/km at the 60-GHz band [9]. This challenge could be tackled by densifying the wireless network and deploying more access points within a relatively small geographical region [10]. However, this densification solution needs the support of a capable infrastructure, one that is relatively low-cost and can handle the huge traffic passing through the network.

A great candidate for such infrastructure is the radio-over-fiber (RoF) networks where mmWave signal is loaded directly over fiber channels, benefiting from the widely deployed

Manuscript received 16 October 2022; accepted 18 October 2022. Date of publication 20 October 2022; date of current version 28 October 2022. This work was supported by the National Plan for Science, Technology and Innovation (MAARIFAH), King Abdulaziz City for Science and Technology, Kingdom of Saudi Arabia, under Grant 2-17-02-001-0009. *(Corresponding author: Amr M. Ragheb.)*

Amr M. Ragheb, Muhammad R. Alrabeiah, and Saleh. A. Alshebeili are with the Department of Electrical Engineering, King Saud University, Riyadh 11421, Saudi Arabia, and also with the KACST-TIC in Radio Frequency and Photonics for the e-Society (RFTONICS), King Saud University (KSU), Riyadh 11421, Saudi Arabia (e-mail: aragheb@ksu.edu.sa; marrabeiah@ksu.edu.sa; dsaleh@ksu.edu.sa).

Q. Tareq and Mohammed Z. M. Khan are with the Optoelectronic Research Laboratory (ORL), Electrical Engineering Department, KFUPM, Dhahran 31261, Saudi Arabia, and also with the Center for Communication Systems and Sensing, KFUPM, Dhahran 31261, Saudi Arabia (e-mail: g201705030@kfupm.edu.sa; zahedmk@kfupm.edu.sa).

Maged. A. Esmail is with the Communications and Networks Engineering Department and Smart Systems Engineering Laboratory, Faculty of Engineering, Prince Sultan University, Riyadh 11586, Saudi Arabia (e-mail: mesmail@psu.edu.sa).

Digital Object Identifier 10.1109/JPHOT.2022.3216228

optical networks, low transmission attenuation, low latency, high transmission rates, and broad-spectrum optical devices. In addition, free-space-optics (FSO) is a license-free technology that is envisioned as a coexistence solution with legacy fiber/RF Infrastructure for the 'last mile' connectivity in 5G and 6G networks [11]. FSO channels can be easily installed where fiber deployment is not feasible. However, signal transmission over FSO links is subject to outdoor environmental conditions. One of these conditions is smoke. Smoke particles in the air can cause signal scattering and hence power loss, specifically for FSO signals, because smoke particles are comparable to the FSO signal wavelength. Using FSO links in industrial cities subject to high pollution is challenging, and system performance investigation is critical before installation. In [12] and [13], authors investigated and modeled the amount of signal attenuation due to smoke particles for FSO links. In [14], the authors found that using a 2 μm wavelength light source is less attenuated by smoke than using 1.5 μm.

Recently, RoF and hybrid RoF/FSO networks were proposed to demonstrate photonics-based mmWave signal generation and transmission [15], [16], [17]. For instance, a hybrid RoF, RoFSO, and wireless (WL) transmission of mmWave signal at 25-GHz was demonstrated in [15]. The system comprises a 5-km single-mode fiber (SMF), 2-m FSO channel, and 3.3-m WL channel. The transmission performance of long-term evolution signal with 4/16/64-quadrature amplitude modulation (QAM) formats were evaluated under various turbulent indoor FSO channels. In [16], a bidirectional RoF architecture was introduced to generate a 60-GHz quadrature amplitude modulation (QPSK) orthogonal frequency division multiplexing (OFDM) signal. The transmission was achieved over 15-km SMF and 0.6-m WL channels. In [17], a RoF communication system of 22.5-km SMF and 1-m WL was proposed to generate and transmit 2/4/8-Gbaud QPSK and 16-QAM signals over 130-GHz mmWave carrier.

In addition, advanced laser sources have been considered extensively as new sources for mmWave signal generation by employing flexible optical heterodyne. Specifically, mmWave signals in the 60-GHz band have been generated by exploiting various lasing methods [18], [19], [20], [21], [22], [23], [24], [25]. For example, a dual-wavelength fiber laser (DWFL) was proposed in [18] using a fiber laser ring cavity to obtain coherent and tunable DWFL with 60 GHz spacing in the 1550 nm region. The transmission performance was assessed using 16-QAM OFDM signal in a RoF architecture of 20 km SMF and 10-m WL channels. In [19], a directly modulated dual-mode laser with dual-mode injection locking in the 1550-nm region has been employed to generate a 60-GHz mmWave signal. The RoF system was evaluated by transmitting a 16-QAM OFDM signal of 6 Gbps over 4-km SMF and 3-m WL channels. Also, a hybrid integrated InP-Si_3N_4 dual laser module, lasing in the 1550-nm region, was considered in [20] to demonstrate a RoF architecture of 10-km SMF and 1-m WL channels. The mmWave signal was obtained in the 60-GHz band, and 64-QAM OFDM signals of 9.84 Gbps were used to evaluate the transmission quality. In [21], a gain-switched distributed feedback laser was employed to generate a 60 GHz mmWave signal. The transmission performance was demonstrated using a 16-QAM OFDM signal of 25 Gbps transmitted over 50 km SMF and 2-m WL channels. Furthermore, very recently, InAs/InP quantum-dash (QD) nanostructure-based lasers have been used extensively as a colorless source for mmWave signal generation in RoF and RoFSO architectures [22]. In [23], [24], the authors demonstrated a C-band QD passively mode-locked laser to generate a 60-GHz mmWave signal of 1.12 Gbps raw data rate in a RoF network of 25-km SMF channel. Also, a C-band QD dual-wavelength distributed feedback laser was demonstrated, in [25], to generate a 60-GHz mmWave signal of 24 Gbps in a RoF architecture of 25.22-km SMF.

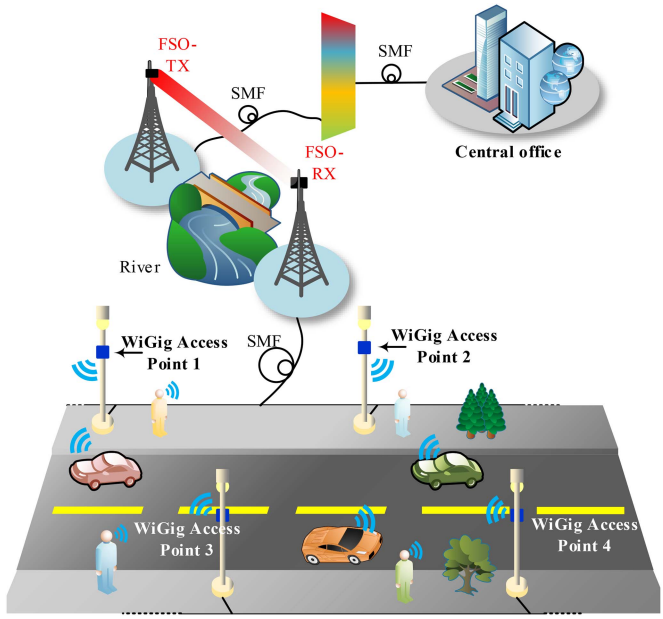

Fig. 1. Architecture of hybrid RoF and RoFSO for WiGig communications. SMF: single mode fiber and FSO: free-space optics.

So far, the above methods generate 60-GHz mmWave signals using matured C-band lasing technologies. To our knowledge, no significant work has yet been reported demonstrating 60-GHz mmWave signal generation and transmission using L-band laser technology. Fig. 1 illustrates a conceptual architecture of the proposed hybrid RoF, RoFSO, and outdoor WiGig access points (APs) architecture where RoF is used in the backhaul to support the WiGig APs with high-speed data rates. When there are obstacles such as rivers and mountains, FSO links are a good alternative. In general, hybrid links that include RoF and FSO are an excellent choice for future WiGig communications. In this paper, we experimentally demonstrate, using an L-band QD laser diode (LD) based mmWave comb source (QD-mmWave), the generation of V-band mmWave signals for high-speed WiGig signals transmission. The performance of the obtained 62.5-GHz mmWave signal is assessed in terms of electrical characteristics and transmission quality. First, the RF phase noise and line-width of the generated mmWave signal are reported. Then, data transmission of 4/6-Gbaud (8/12 Gbps) QPSK is successfully achieved over three different channels; (i) 11.6 km SMF-6 m FSO-2 m WL, (ii) 11.6 km SMF-2 m WL, and (iii) 2 m WL. Moreover, the smoke weather condition effect on the transmitted

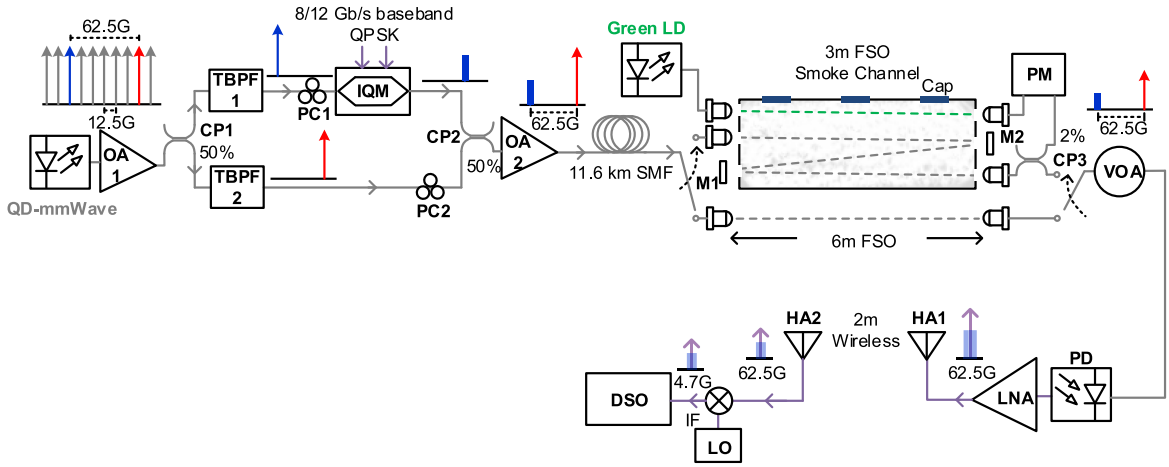

Fig. 2. Experimental setup illustrating different types of transmission channels. QD: quantum-dash laser, mmWave: millimeter-wave, TBPF: tunable bandpass filter, PC: polarization controller, OA: optical amplifier, LD: laser diode, PM: power meter, VOA: variable optical attenuator, PD: photodiode, DSO: digital storage oscilloscope, LNA: low noise amplifier, HA: horn antenna, IQM: in-phase-quadrate modulator, LO: local oscillator, IF: intermediate frequency, SMF: single mode fiber, CP: power splitter and combiner.

signal is investigated experimentally using an indoor chamber designed for this purpose. The visibility range parameter is selected for the analysis, and the results dictate the a value of ∼100-m is required to maintain successful transmission.

The remaining sections are organized as follows. Section II discusses the experimental setup, including generating the V-band carrier using QD LD and the hybrid transmission links. In Section III, we discuss the performance of the generated V-band carrier signal and the obtained results of transmitting a high-speed QPSK signal. In addition, we present the effect of smoke on the transmitted signal using different performance metrics. Finally, we conclude in Section IV.

II. Experimental Setup

The block diagram used in this investigation is illustrated in Fig. 2. A digital storage oscilloscope (DSO, Keysight DSOX 932048) is shown at the right end of the block diagram, which receives the down-converted intermediate frequency (IF) electrical signal for processing after passing through a sub-harmonic mixer (SHM, Virginia Diodes WR15SHM) that is fed by a local oscillator (LO), and the mmWave electrical signal from the horn antenna (HA2, QuinStar QWH-VPRR00 50-75 GHz, 24 dBi gain) at 62.5 GHz. The HA2 (receiver) is fixed on an adjustable stage capable of moving over a distance of 0-2 m in conjunction with an identical HA1 (transmitter), which is fed by a low-noise amplifier (LNA, QuinStar QLW-50754530), with 30-dB gain, that amplifies the mmWave signal received from the photodiode (PD, Finisar XPDV3120R). As shown in Fig. 2, the PD receives an optical signal via a variable optical attenuator (VOA, Agilent N7764 A) fed by two different channel configurations. The first is a fixed 6-m FSO channel, while the second configuration consists of a 3-m FSO channel inside a closed chamber (dimensions 100 cm × 20 cm × 20 cm). To perform measurements under different smoke conditions, i.e., the occurrence of low to dense smoke conditions, an experimental setup with a long observation time is required, which is challenging. In addition, it is not easy to reconduct the measurements under the same conditions in an outdoor environment. Therefore, a controlled indoor environment seems an excellent choice to investigate a communication systemâs performance under smoke conditions [12], [26]. In this work, a chamber is built to examine the performance of the QD-mmWave for WiGig applications under smoke weather conditions. The smoke channel has been established via two free-space collimation packages (Thorlabs F810APC-1550) used to couple the signal to and from the free-space. Also, two optical mirrors (M1 and M2) were used to reflect the optical beam twice to realize a length of 3-m. Increasing the optical path length improves the homogeneity of the smoke within the chamber.

Dry smoke particle generation is achieved using a smoke generator machine, which heats the glycerol-based liquid [13], [14]. Inlets/outlets and fans are used to control the density and distribution of the smoke within the chamber. In this work, the visibility range parameter (V) is exploited to study the impact of smoke on the communication link. This parameter is widely used in the literature to design and analyze optical wireless communication links. It is defined as the range to an object where the visual contrast drops to 2% of the original. When the smoke is dense, the visibility range decreases. To measure the visibility range parameter, an FSO link that includes 550 nm LD (i.e., green laser) and a visible band power detector (Thorlabs S121 C) is installed parallel to the communication link. The visibility range parameter is defined mathematically by [12], [26]:

$$V = -7.4\, L/\log(T), \tag{1}$$

where L is the link distance in km and T is the optical signal transmittance, which is measured using the setup as a ratio of the received signal power with smoke to that of without smoke.

To realize variable visibility inside the chamber, we first fill the chamber with a large amount of smoke. This gives the highest

homogeneous smoke density, which corresponds to the largest signal attenuation. Then, the three window caps of the chamber, shown in Fig. 2, are opened, and the smoke particles start to leave the chamber slowly; thus, decreasing the smoke density in the chamber and eventually disappearing. The change of the smoke particles' density along the propagation link with time provides the possibility to measure the visibility range under different smoke densities.

To measure the output optical power from the chamber, 2% of the output arm of the 98/2% optical coupler (CP3) has been employed and connected to an optical power meter (PM, Thorlabs PM320E), while the other 98% arms serve as the optical signal to the VOA. These configurations receive optical signals from an optical amplifier (OA2, Amonics AEDFAL-EX2-B-FA) via an 11.6 km SMF, which is then connected to the FSO channels via a collimated lens system. Two optical tones coupled via CP2 (50/50 %) serve as the input to the OA2. The in-phase-quadrature modulator (IQM, Fujitsu FTM7977HQA) on the top arm of the transmission system, single-sideband modulates the short-wavelength optical tone (blue, λ_1) as depicted in Fig. 2. A polarization controller (PC1) was utilized at the IQM input to align the short-wavelength polarization with that of the IQMâs input. This optical tone is selected from the amplified (OA1, Amonics AEDFAL-EX2-B-FA) optical spectrum of QD-mmWave after passing through a CP1 (50/50%), using an adjustable bandpass filter (TBPF1, EXFO XTM-50). The bottom arm, i.e., output arm of CP1, on the other hand, is used to choose the other non-modulated long-wavelength optical tone (red, λ_2) from the amplified QD-mmWave optical spectrum as depicted in Fig. 2, with optical tones separation being 62.5 GHz. PC2 was used in the non-modulated carrier path to match the polarization of the modulated and non-modulated carriers. The short-wavelength tone (λ_1) from the upper arm is externally modulated with an 8-12 Gb/s QPSK drive signal, as baseband optical modulation, in IQM using an arbitrary waveform generator (Keysight M8195 A), which is generated under a MATLAB environment using a drive signal generated via $2^{11} - 1$ pseudo-random bit-sequence length.

III. Experimental Results

A. Electrical and Optical Characterization

The QD-mmWave constitutes a bare QD-LD, which can be observed from the bottom inset of Fig. 3. The as-cleaved output power from the device's single facet is coupled into an in-house made lensed SMF. The bare 3Ã800 μm^2 InAs/InP QD-LD consists of a four stack chirped barrier thickness InAs dash in an InGaAlAs asymmetric well structure [22]. Keithley2520 was utilized to probe the Fabry-Perot device (a photograph of the probing station is shown in the central inset of Fig. 3) with a continuous wave current of ∼150 mA (∼1.75Ith where Ith is the threshold current), whose ultra-broadband lasing spectrum was self-injection locked to obtain a single-mode emission of ∼40 dB side-mode-suppression-ratio (SMSR) with low noise and small optical linewidth. Later, a broadband emission of several comb lines (>14 lines) is realized with 12.5 GHz spacing exploiting two cascaded phase modulators (PM1 and PM2)

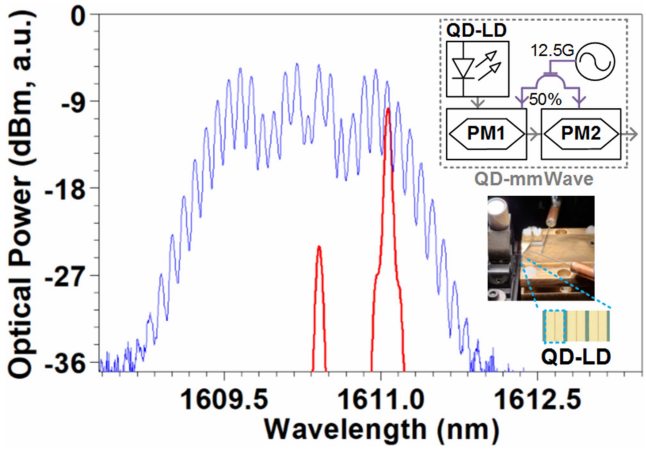

Fig. 3. QD-mmWave source broad spectrum emission. The upper inset shows the block diagram of the QD-mmWave source. The lower inset shows the photograph of the probing station and the bare QD-LD.

driven by a 12.5 GHz RF signal, as shown in the top inset of Fig. 3.

The generated optical spectrum of the QD-mmWave is shown in Fig. 3, which is measured before OA1 using an optical spectrum analyzer (Agilent 86142B, 60 pm resolution), displaying a near-flat top emission with ±1 dB flatness. As shown in the schematic of Fig. 2, two modes, $\lambda_1 = 1610.40$ nm (blue) and $\lambda_2 = 1611.06$ nm (red), corresponding to 62.5 GHz spacing, were selected from the upper and lower arms of the transmitter system, respectively, after passing through OA1 and CP2. However, before initiating the transmission experiment, the electrical characteristics of the non-modulated 62.5 GHz mmWave beat-tone were evaluated by passing the output of CP2 directly into the PD and investigated with an electrical signal analyzer (Keysight N9010B). Owing to the bandwidth limitation of the electrical signal analyzer, the electrical characterization of the mmWave beat-tone was accomplished by down-converting the signal from 62.5 GHz to an IF = 4.7 GHz, and the measured coarse electrical spectrum is depicted in Fig. 4(a). The inset of Fig. 4(a) illustrates the RF linewidth of the mmWave signal under fine resolution, where the −3 dB linewidth of ∼ 1.0 kHz was calculated. Fig. 4(b) plots the measured phase noise parameter of the downconverted mmWave signal, exhibiting superior characteristics. The phase noise was measured to be −45 dBc/Hz and −65 dBc/Hz at 100 Hz at 1 kHz frequency offset. It is noteworthy to mention that the deployed mid L-band QD-mmWave source can potentially be replaced with a mere single section passively mode-locked QD-LD device of appropriate cavity length if mode-locking is observed at the present operating wavelength of ∼1620 nm, which has been matured in the 1550 nm window.

B. 62.5 GHz Mmwave Transmission

The performance of the proposed system is investigated under different channel scenarios and transmission speeds. Fig. 5(a) illustrates the BER performance of a 12 Gb/s QPSK signal transmitted over WL channels. The measurements are taken over three wireless RF channel lengths: 1 m, 1.5 m, and 2 m. In

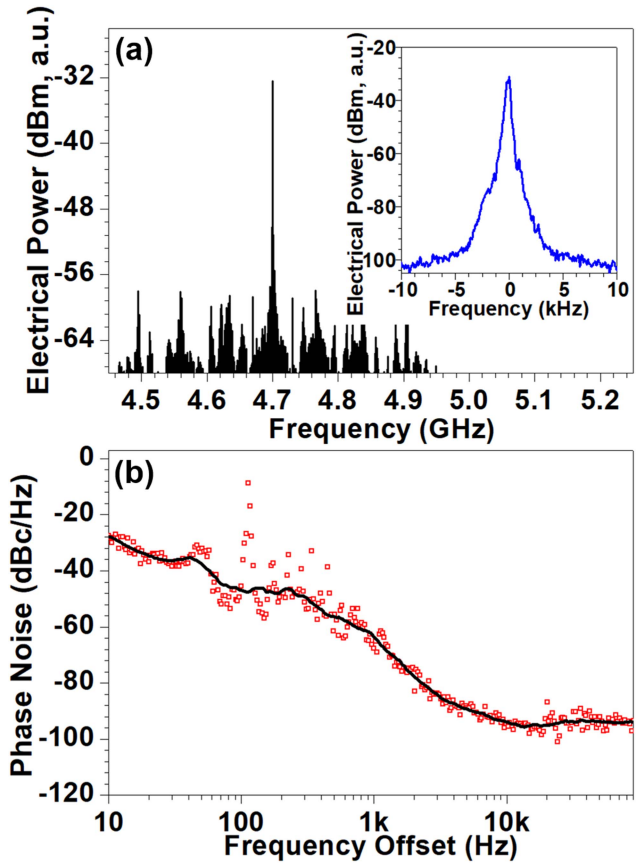

Fig. 4. Electrical characteristics of the downconverted mmWave signal in terms of (a) coarse electrical spectrum and (b) measure phase noise. The inset shows a fine resolution RF spectrum.

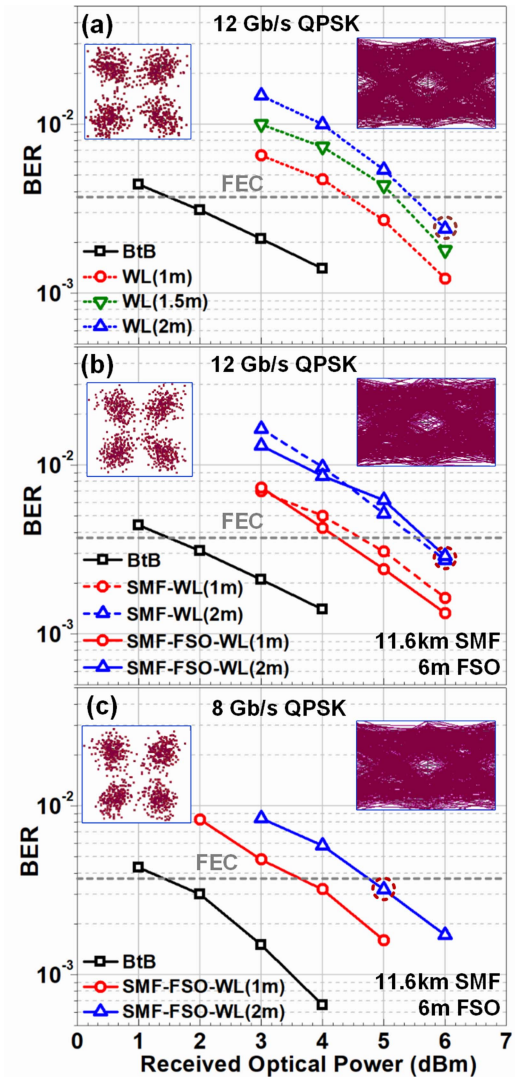

Fig. 5. Performance of the transmission system in terms of BER versus the received optical power for (a) 12 Gb/s QPSK signal and wireless channel, (b) 12 Gb/s QPSK signal and hybrid transmission channel, and (c) 8 Gb/s QPSK signal and hybrid transmission channel.

addition, the measurements are compared with the back-to-back (BtB) configuration when there is no wireless channel. The results show that longer WL channels introduce more attenuation for the transmitted signal, causing higher BERs due to the free-space path loss. Compared to the BtB configuration, the 1-m, 1.5-m, and 2-m WL wireless channels require 3 dB, 3.8 dB, and 4.1 dB more optical power, respectively, to obtain the same BER performance, i.e., FEC limit (BER $= 3.8 \times 10^{-3}$). Fig. 5(a) insets show the signal constellation and eye diagrams corresponding to the 2-m WL link length near the FEC limit (at a received power of 6 dBm).

Next, the performance of the 12 Gb/s QPSK signal is investigated over different hybrid transmission links. This includes 11.6 km SMF-1 m WL hybrid link, 11.6 km SMF-2 m WL hybrid link, 11.6 km SMF- 6 m FSO- 1 m WL hybrid link, and 11.6 km SMF-6 m FSO- 2 m WL hybrid link. The performance of the transmitted signal over different hybrid links in terms of BER is illustrated in Fig. 5(b). Similar to the results in Fig. 5(a), longer WL links cause more power loss and hence higher BER, due to the free-space path loss. When FSO links are introduced, a slight power loss of ∼0.1–0.2 dB is observed. This loss is attributed to the light collimation into the SMF at the FSO link receiver side. It is worth to mention that the loss in optical power caused by adding either the SMF channel (∼ 3 dB) or SMF-FSO channel (∼9 dB) was compensated in the second EDFA (OA2) shown in Fig. 2, to attain the same received optical power range for a fair comparison with the WL case shown in Fig. 5(a). In general, the results show the capability of the proposed system in Fig. 2 to support the transmission of high-speed signals using a QD-mmWave source over hybrid links. The constellation and eye diagrams show the signal performance at the FEC limit demonstrating well separated all the four clustered group and visible open eyes, respectively

The scenario in Fig. 5(b) is repeated in Fig. 5(c) but with a lower-speed transmission signal, i.e., 8 Gb/s. In comparing the performance of the 8 Gb/s and 12 Gb/s QPSK signals, we notice that for the same BER (FEC limit) and 11.6 km SMF-6 m FSO-1 m WL hybrid link, the 12 Gb/s QPSK signal requires ∼0.8 dB more optical power. Moreover, when the WL link increases to 2-m, ∼1 dB extra power loss is needed to reach the same FEC limit. It is worth noting that the transmission performance of the individual WL and SMF-WL channels at 8 Gb/s speed will

show a slight difference in the optical receiver sensitivity with respect to the whole hybrid channel (SMF-FSO-WL); this has been concluded from the results shown in Fig. 5(a) and (b) for the 12 Gb/s case. The constellation and eye diagrams of the 2-m WL RoF and RoFSO link show successful received signal performance near the FEC limit. In general, higher data rates require more optical power to achieve successful transmission than the lower data rates which are ascribed to the deployed system's equipment and optical and electrical component bandwidth limitations.

C. 62.5 GHz Mmwave Transmission Under Smoky Channel

The discussion in the previous subsection was dedicated to a clear free-space indoor channel. In this subsection, we investigate the effect of smoke particles on the signal's transmission performance. When the optical signal propagates in free-space, the smoke particles cause signal scattering, yielding power loss (attenuation) at the receiver. The severity of the attenuation depends on the smoke density. Such density can be expressed in terms of visibility range and specific signal attenuation parameters, as has been applied to the dust environment in literature [26]. In the subsequent analysis, we considered 12 Gb/s QPSK signal transmission over 11.6 km SMF, 3 m FSO smoke channel, and 0.1 m WL link length. The received optical power at PD was measured to be 5.7 dBm with an EVM of ∼22% before injecting smoke into the chamber. It is worth mentioning that the smoke channel exhibited ∼1.5 dB higher channel loss compared to the 6 m clear weather FSO link. Hence the required received optical power, in the present scenario, to reach the EVM value as mentioned above, is expected to be larger than the clear weather transmission results.

Fig. 6 illustrates the performance of a 12 Gb/s QPSK signal in terms of the visibility range. The visibility range reduces for the high density of smoke particles. Four performance metrics are considered here; BER, error vector magnitude (EVM), signal-to-noise ratio (SNR), and received electrical power. It is clear from Fig. 6(a) that the BER increases for the low visibility range due to signal power loss. The FEC limit is achieved at about a 100-m visibility range. This value of visibility range corresponds to 37% EVM and 8.5 dB SNR. Such values ensure the successful transmission of the 12 Gbps QPSK signal under the examined smoke channel [27]. Therefore, for the setup proposed in Fig. 2, the visibility range should be at least 100-m to successfully transmit a 12 Gb/s QPSK signal. The insets in Fig. 6(a) (top right) show the signal constellation and eye diagram at poor performance, i.e., low visibility range, while the insets in Fig. 6(a) (bottom left) show good performance, i.e., large visibility range.

In Fig. 6(b), the investigation is carried out regarding the EVM and SNR metrics. Similar to BER, the EVM value decreases for the high visibility range because of less power loss. On the other side, the SNR value improves for higher values of visibility range due to signal power improvement. In these cases, the FEC limit is also achieved at about 100-m visibility range, thus corroborating well with the calculated value from Fig. 6(a). The effect of the visibility range on the received

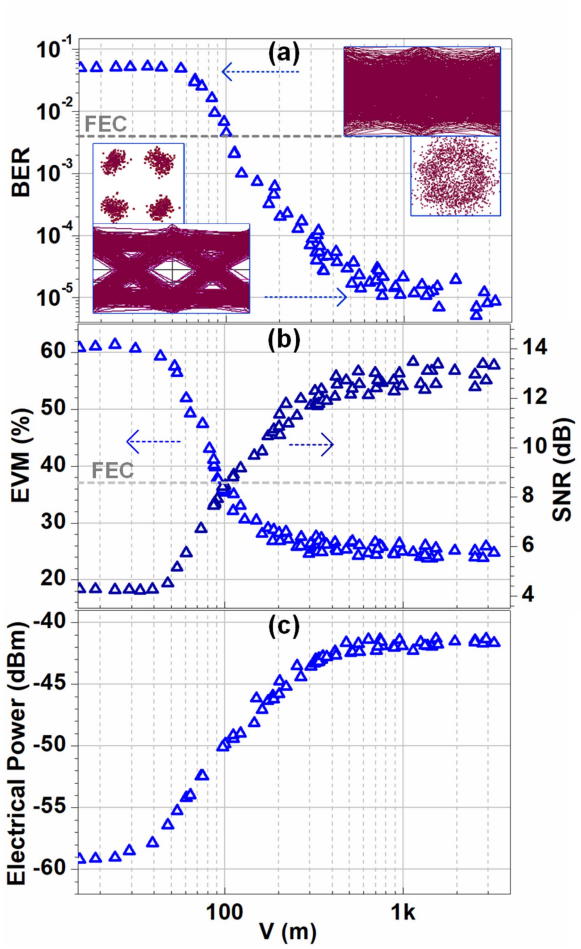

Fig. 6. Performance of the transmission system in terms of visibility range versus (a) BER, (b) EVM%, and (c) electrical power.

electrical power is depicted in Fig. 6(c). The curve shows clearly that the received power improves for higher values of the visibility range.

The specific signal attenuation is a valuable parameter to be considered in FSO communications. It is used in planning the free-space link budget, which defines the amount of power loss in dB/km. In Fig. 7, the performance of the 12 Gbps QPSK is investigated as a function of the signal visibility range, BER, and EVM, versus the specific signal attenuation parameter. Fig. 7(a) indicates the visibility range in meters versus the specific signal attenuation in dB/km. For instance, a 1000-m visibility range expresses a 100-dB/km specific signal attenuation. When the visibility range reduces to 100-m, the specific signal attenuation increases around ten times.

The system performance in terms of SNR and EVM is indicated in Fig. 7(b). Since the increase of the specific signal attenuation parameter means more power loss, the SNR decreases while EVM increases. In this case, the FEC limit corresponds to around ∼900–1000 dB/km specific signal attenuation. Similarly, the BER results are illustrated in Fig. 7(c), where the FEC limit is achieved for around the same value of the specific signal attenuation, i.e., ∼900–1000 dB/km.

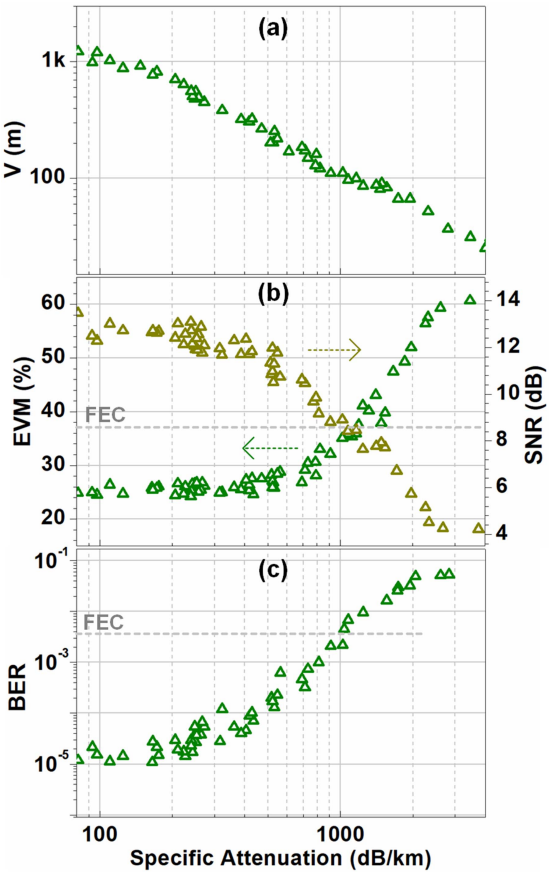

Fig. 7. Performance of the transmission system in terms of specific attenuation versus (a) visibility range, (b) EVM%, and (c) BER.

IV. Conclusion

This paper proposed the generation of a 62.5-GHz mmWave signal using a mid L-band QD LD based mmWave comb source. First, electrical characterizations were performed on the generated mmWave signal in terms of measured RF linewidth and phase noise, exhibiting small values and thus affirming quality mmWave carrier signal generation. Then, a 12 Gbps QPSK mmWave signal was successfully communicated over various transmission mediums comprising 11.6-km SMF, 6-m FSO, and 2-m WL. A worst-case receiver sensitivity of 5.5 dBm was required under the hybrid channel to achieve the BER-FEC limit. Also, the effect of various densities of smoke FSO channel on the quality of the 62.5-GHz 12 Gbps mmWave signal was investigated. Around 100-m free-space visibility range was found to achieve successful transmission under an indoor controlled smoky channel environment.

References

[1] CISCO, "Cisco annual internet report (2018-2023)," San Jose, CA, USA, CISCO, Tech. Rep. 3, 2020.

[2] T. S. Rappaport et al., "Wireless communications and applications above 100 GHz: Opportunities and challenges for 6G and beyond," *IEEE Access*, vol. 7, pp. 78729–78757, 2019.

[3] Y. Xing, T. S. Rappaport, and A. Ghosh, "Millimeter wave and sub-THz indoor radio propagation channel measurements, models, and comparisons in an office environment," *IEEE Commun. Lett.*, vol. 25, no. 10, pp. 3151–3155, Oct. 2021.

[4] Y. Ghasempour, C. R. C. M. da Silva, C. Cordeiro, and E. W. Knightly, "IEEE 802.11ay: Next-generation 60 GHz communication for 100 Gb/s Wi-Fi," *IEEE Commun. Mag.*, vol. 55, no. 12, pp. 186–192, Dec. 2017.

[5] C. J. Hansen, "WiGiG: Multi-gigabit wireless communications in the 60 GHz band," *IEEE Wireless Commun.*, vol. 18, no. 6, pp. 6–7, Dec. 2011.

[6] E. M. Mohamed, M. A. Abdelghany, and M. Zareei, "An efficient paradigm for multiband WiGig D2D networks," *IEEE Access*, vol. 7, pp. 70032–70045, 2019.

[7] I. Ahmed, H. Khammari, M. K. Shahid, and A. Nawaz, "Crowd management using low energy mmwave WiGig with point-to-massive-points communications," in *Proc. Adv. Sci. Eng. Technol. Int. Conf.*, 2020, pp. 1–5.

[8] R. W. Heath, N. González-Prelcic, S. Rangan, W. Roh, and A. M. Sayeed, "An overview of signal processing techniques for millimeter wave MIMO systems," *IEEE J. Sel. Topics Signal Process.*, vol. 10, no. 3, pp. 436–453, Apr. 2016.

[9] T. Yilmaz, E. Fadel, and O. B. Akan, "Employing 60 Ghz ISM band for 5G wireless communications," in *Proc. IEEE Int. Black Sea Conf. Commun. Netw.*, 2014, pp. 77–82.

[10] T. S. Rappaport et al., "Millimeter wave mobile communications for 5G cellular: It will work!," *IEEE Access*, vol. 1, pp. 335–349, 2013.

[11] A. Trichili et al., "Retrofitting FSO systems in existing RF infrastructure: A non-zero-sum game technology," *IEEE Open J. Commun. Soc.*, vol. 2, pp. 2597–2615, 2021.

[12] M. Ijaz, Z. Ghassemlooy, J. Pesek, O. Fiser, H. Le Minh, and E. Bentley, "Modeling of fog and smoke attenuation in free space optical communications link under controlled laboratory conditions," *J. Lightw. Technol.*, vol. 31, no. 11, pp. 1720–1726, Jun. 2013.

[13] M. Ijaz, Z. Ghassemlooy, H. Le Minh, S. Rajbhandari, and J. Perez, "Analysis of fog and smoke attenuation in a free space optical communication link under controlled laboratory conditions," in *Proc. Int. Workshop Opt. Wireless Commun.*, 2012, pp. 1–3.

[14] P. Lin, T. Wang, W. Ma, Q. Yang, and Z. Liu, "Transmission characteristics of 1.55 and 2.04 μm laser carriers in a simulated smoke channel based on an actively mode-locked fiber laser," *Opt. Exp.*, vol. 28, no. 26, pp. 39216–39226, Dec. 2020.

[15] D.-N. Nguyen, J. Bohata, M. Komanec, S. Zvanovec, B. Ortega, and Z. Ghassemlooy, "Seamless 25 GHz transmission of LTE 4/16/64-QAM signals over hybrid SMF/FSO and wireless link," *J. Lightw. Technol.*, vol. 37, no. 24, pp. 6040–6047, Dec. 2019.

[16] B. Wu et al., "Polarization-insensitive remote access unit for radio-over-fiber mobile fronthaul system by reusing polarization orthogonal light waves," *IEEE Photon. J.*, vol. 8, no. 1, Feb. 2016, Art. no. 7200108.

[17] J. L. Li, F. Zhao, and J. Yu, "D-band millimeter wave generation and transmission though radio-over-fiber system," *IEEE Photon. J.*, vol. 12, no. 2, pp. 1–8, Apr. 2020.

[18] S. Alavi, M. Soltanian, I. Amiri, M. Khalily, A. Supa'at, and H. Ahmad, "Towards 5G: A photonic based millimeter wave signal generation for applying in 5G access fronthaul," *Sci. Rep.*, vol. 6, no. 1, pp. 1–11, 2016.

[19] C.-T. Tsai, C.-H. Lin, C.-T. Lin, Y.-C. Chi, and G.-R. Lin, "60-GHz millimeter-wave over fiber with directly modulated dual-mode laser diode," *Sci. Rep.*, vol. 6, no. 1, pp. 1–12, 2016.

[20] D. Dass, A. Delmade, L. Barry, C. G. Roeloffzen, D. Geuzebroek, and C. Browning, "Flexible V-band mmwave analog-RoF transmission of 5G and WiGig signals using an InP-SiN integrated laser module," in *Proc. Int. Topical Meeting Microw. Photon.*, 2021, pp. 1–4.

[21] E. P. Martin et al., "25-Gb/s OFDM 60-GHz radio over fiber system based on a gain switched laser," *J. Lightw. Technol.*, vol. 33, no. 8, pp. 1635–1643, Apr. 2015.

[22] M. Z. M. Khan, "Quantum-dash laser-based tunable 50/75 GHz mmW transport system for future L-band networks," *IEEE Photon. Technol. Lett.*, vol. 34, no. 16, pp. 842–845, Aug. 2022.

[23] A. Delmade et al., "Quantum dash passively mode locked laser for optical heterodyne millimeter-wave analog radio-over-fiber fronthaul systems," in *Proc. Opt. Fiber Commun. Conf. Exhibit.*, 2020, pp. 1–3.

[24] A. Delmade et al., "Optical heterodyne analog radio-over-fiber link for millimeter-wave wireless systems," *J. Lightw. Technol.*, vol. 39, no. 2, pp. 465–474, Jan. 2021.

[25] K. Zeb et al., "A quantum-dash dual-wavelength DFB laser for optical millimeter-wave radio-over-fiber systems," in *Proc. Opt. Fiber Commun. Conf.*, 2021, pp. 1–3.

[26] M. A. Esmail, H. Fathallah, and M.-S. Alouini, "An experimental study of FSO link performance in desert environment," *IEEE Commun. Lett.*, vol. 20, no. 9, pp. 1888–1891, Sep. 2016.

[27] R. A. Shafik, M. S. Rahman, and A. R. Islam, "On the extended relationships among EVM, BER and SNR as performance metrics," in *Proc. Int. Conf. Elect. Comput. Eng.*, 2006, pp. 408–411.